

Meron-Cluster Simulation of a Chiral Phase Transition with Staggered Fermions *

S. Chandrasekharan^a, J. Cox^b, K. Holland^b and U.-J. Wiese^b

^a Department of Physics
Duke University
Durham, North Carolina 27708, U.S.A.

^b Center for Theoretical Physics,
Laboratory for Nuclear Science and Department of Physics
Massachusetts Institute of Technology (MIT)
Cambridge, Massachusetts 02139, U.S.A.

DUKE-TH-99-189, MIT-CTP-2876

February 1, 2008

Abstract

We examine a $(3+1)$ -dimensional model of staggered lattice fermions with a four-fermion interaction and $\mathbf{Z}(2)$ chiral symmetry using the Hamiltonian formulation. This model cannot be simulated with standard fermion algorithms because those suffer from a very severe sign problem. We use a new fermion simulation technique — the meron-cluster algorithm — which solves the sign problem and leads to high-precision numerical data. We investigate the finite temperature chiral phase transition and verify that it is in the universality class of the 3-d Ising model using finite-size scaling.

*This work is supported in part by funds provided by the U.S. Department of Energy (D.O.E.) under cooperative research agreements DE-FC02-94ER40818 and DE-FG02-96ER40945.

1 Introduction

The numerical simulation of lattice fermions is a notoriously difficult problem which is the major stumbling block in solving QCD and other fermionic field theories. The standard method is to integrate out the fermions and to simulate the resulting bosonic problem with a non-local action. In several cases of physical interest — for example, for QCD with an odd number of flavors or with non-zero chemical potential — the bosonic Boltzmann factor may become negative or even complex and thus cannot be interpreted as a probability. When the sign or the complex phase of the Boltzmann factor is included in measured observables, the numerical simulation suffers from severe cancellations resulting in a sign problem. The standard fermion algorithms are incapable of exploring such models. As a consequence, QCD is usually simulated with an even number of flavors and at zero chemical potential. Even in the absence of a sign problem, the simulation of fermions is difficult. For example, lattice QCD simulations suffer from critical slowing down when one approaches the chiral limit in which the quarks become massless. In particular, this makes it difficult to identify the universality class of the finite temperature QCD chiral phase transition.

Even in simpler models with four-fermion interactions the identification of the finite temperature critical behavior is a non-trivial issue [1]. A model with N fermion flavors shows mean-field behavior in the $N = \infty$ limit. On the other hand, at finite N one finds the non-trivial critical behavior that one expects based on dimensional reduction and standard universality arguments. For example, in [2] it has been verified that the chiral phase transition in a $(2 + 1)$ -d four-fermion model with $N = 4$ and $\mathbf{Z}(2)$ chiral symmetry is in the universality class of the 2-d Ising model. Due to the fermion sign problem, standard fermion simulation methods often do not work in models with a too small number of flavors.

In this paper we apply a recently developed technique [3] for solving the sign problem to a $(3 + 1)$ -d model of staggered fermions using the Hamiltonian formulation. The model has $N = 2$ flavors and a $\mathbf{Z}(2)$ chiral symmetry that is spontaneously broken at low temperatures. The fermion determinant can be negative in this model. Hence, due to the sign problem standard fermion algorithms fail in this case. Our algorithm is the only numerical method available to simulate this model. In this method we do not integrate out the fermions but describe them in a Fock state basis. The resulting bosonic model of fermion occupation numbers interacts locally, but has a non-local fermion permutation sign resulting from the Pauli exclusion principle. Standard numerical methods would suffer from severe cancellations of positive and negative contributions to the partition function. Like other cluster methods, our algorithm decomposes a configuration of fermion occupation numbers into clusters which can be flipped independently. Under a cluster flip an occupied site becomes empty and vice versa. The main idea of the meron-cluster algorithm is to construct the clusters such that they affect the fermion sign independent of each other when they are flipped. In addition, it must always be possible to flip the clusters into a ref-

erence configuration with a positive sign. A cluster whose flip changes the fermion sign is referred to as a meron because it can be viewed as a half-instanton. If a configuration contains a meron-cluster, its contribution to the partition function is canceled by the contribution of the configuration that one obtains when the meron-cluster is flipped. The observables that we consider get non-zero contributions from the zero- and two-meron sectors only. Our algorithm ensures that configurations with more than two merons are never generated, which leads to an exponential gain in statistics and to a complete solution of the sign problem.

Like other cluster algorithms the meron algorithm substantially reduces critical slowing down. This allows us to work directly in the chiral limit. As a result, we can study the nature of the chiral phase transition in great detail. The $\mathbf{Z}(2)$ chiral symmetry is spontaneously broken at low temperatures and gets restored in the high-temperature phase. As expected, the system close to the finite temperature critical point is in the universality class of the 3-d Ising model. We verify this in a high-precision finite-size scaling investigation of the chiral susceptibility.

The paper is organized as follows. In section 2 we introduce the staggered fermion Hamiltonian, derive the path integral representation of the partition function, and discuss the fermion sign as well as relevant observables. Section 3 contains the description of the meron-cluster algorithm and the corresponding improved estimators. In section 4, we present the results of numerical simulations and extract the critical behavior from the finite-size scaling of the chiral susceptibility. Finally, section 5 contains our conclusions.

2 The Staggered Fermion Model

Let us consider staggered fermions hopping on a 3-d cubic spatial lattice with $V = L^3$ sites x (L even) and with periodic or antiperiodic spatial boundary conditions. We start in the Hamiltonian formulation and then derive a path integral on a $(3+1)$ -d Euclidean space-time lattice. The fermions are described by creation and annihilation operators Ψ_x^+ and Ψ_x with standard anticommutation relations

$$\{\Psi_x^+, \Psi_y^+\} = \{\Psi_x, \Psi_y\} = 0, \quad \{\Psi_x^+, \Psi_y\} = \delta_{xy}. \quad (2.1)$$

The staggered fermion Hamilton operator takes the form

$$H = \sum_{x,i} h_{x,i} + m \sum_x (-1)^{x_1+x_2+x_3} \Psi_x^+ \Psi_x, \quad (2.2)$$

that is a sum of nearest-neighbor couplings $h_{x,i}$ and a mass term $m\bar{\Psi}\Psi$. In the following we work directly in the chiral limit, $m = 0$, and only use $\bar{\Psi}\Psi$ as an observable. The term $h_{x,i}$ couples the fermion operators at the lattice sites x and

$x + \hat{i}$, where \hat{i} is a unit-vector in the i -direction, and

$$h_{x,i} = \frac{1}{2}\eta_{x,i}(\Psi_x^+ \Psi_{x+\hat{i}} + \Psi_{x+\hat{i}}^+ \Psi_x) + G(\Psi_x^+ \Psi_x - \frac{1}{2})(\Psi_{x+\hat{i}}^+ \Psi_{x+\hat{i}} - \frac{1}{2}). \quad (2.3)$$

Here $\eta_{x,1} = 1$, $\eta_{x,2} = (-1)^{x_1}$ and $\eta_{x,3} = (-1)^{x_1+x_2}$ are the standard staggered fermion sign factors, and G is a four-fermion coupling constant. The system has a conserved fermion number

$$N = \sum_x \Psi_x^+ \Psi_x, \quad (2.4)$$

because $[H, N] = 0$. Besides the $U(1)$ fermion number symmetry, the model has a $\mathbf{Z}(2)$ chiral symmetry, which (up to a phase) simply shifts Ψ_x^+ and Ψ_x by one lattice spacing in all three directions. This changes the sign of $\bar{\Psi}\Psi$ but leaves the $m = 0$ Hamiltonian invariant. There are also other $\mathbf{Z}(2)$ symmetries which correspond to discrete flavor transformations. For a detailed discussion of the symmetries of staggered fermions in the Hamiltonian formulation we refer to [4].

To construct a path integral for the partition function, we decompose the Hamilton operator into six terms $H = H_1 + H_2 + \dots + H_6$, with

$$H_i = \sum_{\substack{x=(x_1,x_2,x_3) \\ x_i \text{ even}}} h_{x,i}, \quad H_{i+3} = \sum_{\substack{x=(x_1,x_2,x_3) \\ x_i \text{ odd}}} h_{x,i}. \quad (2.5)$$

The individual contributions to a given H_i commute with each other, but two different H_i do not commute. Using the Suzuki-Trotter formula we express the fermionic partition function at inverse temperature β as

$$Z_f = \text{Tr}[\exp(-\beta H)] = \lim_{M \rightarrow \infty} \text{Tr}[\exp(-\epsilon H_1) \exp(-\epsilon H_2) \dots \exp(-\epsilon H_6)]^M. \quad (2.6)$$

We have introduced $6M$ Euclidean time slices with $\epsilon = \beta/M$ being the lattice spacing in the Euclidean time direction. Following Jordan and Wigner [5] we represent the fermion operators by Pauli matrices

$$\Psi_x^+ = \sigma_1^3 \sigma_2^3 \dots \sigma_{l-1}^3 \sigma_l^+, \quad \Psi_x = \sigma_1^3 \sigma_2^3 \dots \sigma_{l-1}^3 \sigma_l^-, \quad n_x = \Psi_x^+ \Psi_x = \frac{1}{2}(\sigma_l^3 + 1), \quad (2.7)$$

with

$$\sigma_l^\pm = \frac{1}{2}(\sigma_l^1 \pm i\sigma_l^2), \quad [\sigma_l^i, \sigma_m^j] = 2i\delta_{lm}\epsilon_{ijk}\sigma_l^k. \quad (2.8)$$

Here l labels the lattice point x . The Jordan-Wigner representation requires an ordering of the lattice points. For example, one can label the point $x = (x_1, x_2, x_3)$ (with $x_i = 0, 1, \dots, L-1$) by $l = 1 + x_1 + x_2 L + x_3 L^2$. It should be pointed out that the Jordan-Wigner representation works in any dimension. In one dimension the lattice points are, of course, naturally ordered, but even in higher dimensions the physics is completely independent of the arbitrary ordering. We now insert complete sets of fermion Fock states between the factors $\exp(-\epsilon H_i)$. Each site is either empty or occupied, i.e. n_x has eigenvalue 0 or 1. In the Pauli matrix representation this

corresponds to eigenstates $|0\rangle$ and $|1\rangle$ of σ_l^3 with $\sigma_l^3|0\rangle = -|0\rangle$ and $\sigma_l^3|1\rangle = |1\rangle$. The transfer matrix is a product of factors

$$\exp(-\epsilon h_{x,i}) = \exp\left(\frac{\epsilon G}{4}\right) \begin{pmatrix} \exp(-\frac{\epsilon G}{2}) & 0 & 0 & 0 \\ 0 & \cosh \frac{\epsilon}{2} & \Sigma \sinh \frac{\epsilon}{2} & 0 \\ 0 & \Sigma \sinh \frac{\epsilon}{2} & \cosh \frac{\epsilon}{2} & 0 \\ 0 & 0 & 0 & \exp(-\frac{\epsilon G}{2}) \end{pmatrix}, \quad (2.9)$$

which is a 4×4 matrix in the Fock space basis $|00\rangle$, $|01\rangle$, $|10\rangle$ and $|11\rangle$ of two sites x and $x + \hat{i}$. Here $\Sigma = \eta_{x,i} \sigma_{l+1}^3 \sigma_{l+2}^3 \dots \sigma_{m-1}^3$ includes the local sign $\eta_{x,i}$ as well as a non-local string of Pauli matrices running over consecutive labels between l and m , where l labels the lattice point x and m labels $x + \hat{i}$. Note that Σ is diagonal in the occupation number basis.

The partition function is now expressed as a path integral

$$Z_f = \sum_n \text{Sign}[n] \exp(-S[n]), \quad (2.10)$$

over configurations of occupation numbers $n(x, t) = 0, 1$ on a $(3 + 1)$ -d space-time lattice of points (x, t) . The Boltzmann factor

$$\begin{aligned} \exp(-S[n]) &= \prod_{\substack{x=(x_1, x_2, x_3) \\ x_1 \text{ even}, t=6m}} \exp\{-s[n(x, t), n(x + \hat{1}, t), n(x, t + 1), n(x + \hat{1}, t + 1)]\} \\ &\times \prod_{\substack{x=(x_1, x_2, x_3) \\ x_2 \text{ even}, t=6m+1}} \exp\{-s[n(x, t), n(x + \hat{2}, t), n(x, t + 1), n(x + \hat{2}, t + 1)]\} \\ &\times \prod_{\substack{x=(x_1, x_2, x_3) \\ x_3 \text{ even}, t=6m+2}} \exp\{-s[n(x, t), n(x + \hat{3}, t), n(x, t + 1), n(x + \hat{3}, t + 1)]\} \\ &\times \prod_{\substack{x=(x_1, x_2, x_3) \\ x_1 \text{ odd}, t=6m+3}} \exp\{-s[n(x, t), n(x + \hat{1}, t), n(x, t + 1), n(x + \hat{1}, t + 1)]\} \\ &\times \prod_{\substack{x=(x_1, x_2, x_3) \\ x_2 \text{ odd}, t=6m+4}} \exp\{-s[n(x, t), n(x + \hat{2}, t), n(x, t + 1), n(x + \hat{2}, t + 1)]\} \\ &\times \prod_{\substack{x=(x_1, x_2, x_3) \\ x_3 \text{ odd}, t=6m+5}} \exp\{-s[n(x, t), n(x + \hat{3}, t), n(x, t + 1), n(x + \hat{3}, t + 1)]\}, \end{aligned} \quad (2.11)$$

(with $m = 0, 1, \dots, M - 1$) is a product of space-time plaquette contributions with

$$\begin{aligned} \exp(-s[0, 0, 0, 0]) &= \exp(-s[1, 1, 1, 1]) = \exp(-\frac{\epsilon G}{2}), \\ \exp(-s[0, 1, 0, 1]) &= \exp(-s[1, 0, 1, 0]) = \cosh \frac{\epsilon}{2}, \\ \exp(-s[0, 1, 1, 0]) &= \exp(-s[1, 0, 0, 1]) = \sinh \frac{\epsilon}{2}. \end{aligned} \quad (2.12)$$

All the other Boltzmann weights are zero, which implies several constraints on allowed configurations. Note that here we have dropped the trivial overall factor $\exp(\epsilon G/4)$ that appeared in eq.(2.9).

The sign of a configuration, $\text{Sign}[n]$, also is a product of space-time plaquette contributions $\text{sign}[n(x, t), n(x + \hat{i}, t), n(x, t + 1), n(x + \hat{i}, t + 1)]$ with

$$\begin{aligned}\text{sign}[0, 0, 0, 0] &= \text{sign}[0, 1, 0, 1] = \text{sign}[1, 0, 1, 0] = \text{sign}[1, 1, 1, 1] = 1, \\ \text{sign}[0, 1, 1, 0] &= \text{sign}[1, 0, 0, 1] = \Sigma.\end{aligned}\tag{2.13}$$

It should be noted that Σ gets contributions from all lattice points with labels between l and m . This seems to make an evaluation of the fermion sign rather tedious. Also, it is not a priori obvious that $\text{Sign}[n]$ is independent of the arbitrarily chosen order of the lattice points. Fortunately, there is a simple way to compute $\text{Sign}[n]$, which is directly related to the Pauli exclusion principle and which is manifestly order-independent. In fact, $\text{Sign}[n]$ has a topological meaning. The occupied lattice sites define fermion world-lines which are closed around the Euclidean time direction. Of course, during their Euclidean time evolution fermions can interchange their positions, and the fermion world-lines define a permutation of particles. The Pauli exclusion principle dictates that the fermion sign is just the sign of that permutation. If we work with antiperiodic spatial boundary conditions, $\text{Sign}[n]$ receives an extra minus-sign for every fermion world-line that crosses a spatial boundary. Figure 1 shows two configurations of fermion occupation numbers in $(1 + 1)$ dimensions. The first configuration corresponds to two fermions at rest and has $\text{Sign}[n] = 1$. In the second configuration two fermions interchange their positions with one fermion stepping over the spatial boundary. If one uses periodic spatial boundary conditions this configuration has $\text{Sign}[n] = -1$. Note that the same configuration would have $\text{Sign}[n] = 1$ when antiperiodic boundary conditions are used.

The expectation value of a fermionic observable $O[n]$ is given by

$$\langle O \rangle_f = \frac{1}{Z_f} \sum_n O[n] \text{Sign}[n] \exp(-S[n]).\tag{2.14}$$

Quantities of physical interest are the chiral condensate

$$\bar{\Psi}\Psi[n] = \frac{\epsilon}{6} \sum_{x,t} (-1)^{x_1+x_2+x_3} (n(x, t) - \frac{1}{2}),\tag{2.15}$$

and the corresponding chiral susceptibility

$$\chi = \frac{1}{\beta V} \langle (\bar{\Psi}\Psi)^2 \rangle_f.\tag{2.16}$$

Up to now we have derived a path integral representation for the fermion system in terms of bosonic occupation numbers and a fermion sign factor that encodes Fermi

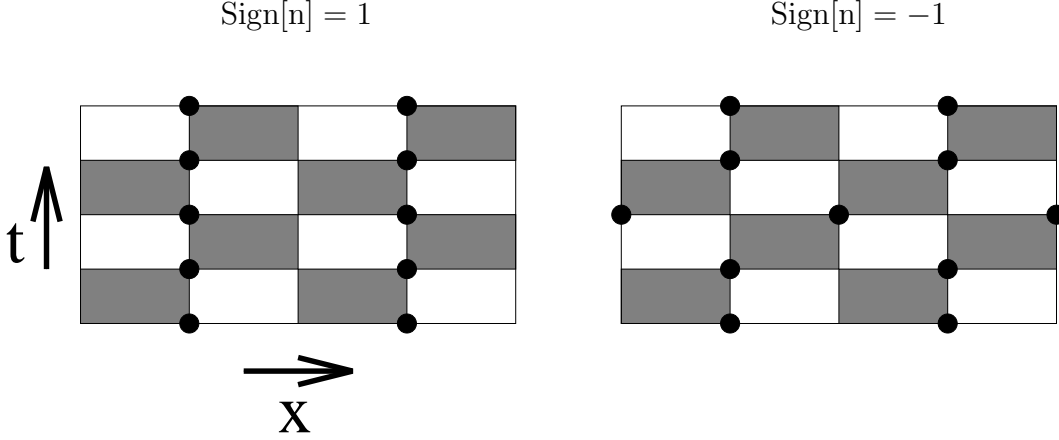


Figure 1: *Two configurations of fermion occupation numbers in $(1+1)$ dimensions. The shaded plaquettes carry the interaction. The dots represent occupied sites. In the second configuration two fermions interchange their positions. With periodic spatial boundary conditions this configuration has $\text{Sign}[n] = -1$.*

statistics. The system without the sign factor is bosonic and is characterized by the positive Boltzmann factor $\exp(-S[n])$. Here the bosonic model is a quantum spin system with the Hamiltonian

$$H = \sum_{x,i} (S_x^1 S_{x+\hat{i}}^1 + S_x^2 S_{x+\hat{i}}^2 + G S_x^3 S_{x+\hat{i}}^3), \quad (2.17)$$

where $S_x^i = \frac{1}{2}\sigma_l^i$ is a spin 1/2 operator associated with the lattice site x that was labeled by l . The case $G = 1$ corresponds to the isotropic antiferromagnetic quantum Heisenberg model, $G = 0$ represents the quantum XY-model, and $G = -1$ corresponds to an isotropic ferromagnet. In the language of the spin model, the chiral condensate turns into the staggered magnetization

$$\overline{\Psi}\Psi = \frac{\epsilon}{6} \sum_{x,t} (-1)^{x_1+x_2+x_3} S_x^3. \quad (2.18)$$

For sufficiently large G , for example in an antiferromagnet with $G = 1$, the staggered magnetization gets a non-zero expectation value at sufficiently low temperature, thus breaking the bosonic analog of chiral symmetry. It will turn out that the fermion sign does not change this behavior, and indeed chiral symmetry is spontaneously broken in the fermionic model as well.

3 The Meron-Cluster Algorithm

Let us first discuss the nature of the fermion sign problem. The fermionic path integral $Z_f = \sum_n \text{Sign}[n] \exp(-S[n])$ includes the fermion sign factor $\text{Sign}[n] = \pm 1$

as well as a positive Boltzmann factor $\exp(-S[n])$ that contains the action $S[n]$ of the corresponding bosonic model with partition function $Z_b = \sum_n \exp(-S[n])$. A fermionic observable $O[n]$ is obtained in a simulation of the bosonic ensemble as

$$\langle O \rangle_f = \frac{1}{Z_f} \sum_n O[n] \text{Sign}[n] \exp(-S[n]) = \frac{\langle O \text{Sign} \rangle}{\langle \text{Sign} \rangle}. \quad (3.1)$$

The average sign in the simulated bosonic ensemble is given by

$$\langle \text{Sign} \rangle = \frac{1}{Z_b} \sum_n \text{Sign}[n] \exp(-S[n]) = \frac{Z_f}{Z_b} = \exp(-\beta V \Delta f). \quad (3.2)$$

The last equality points to the heart of the sign problem. The expectation value of the sign is exponentially small in both the volume V and the inverse temperature β because the difference between the free energy densities $\Delta f = f_f - f_b$ of the fermionic and bosonic systems is necessarily positive.

Even in an ideal simulation of the bosonic ensemble which generates N completely uncorrelated configurations, the relative statistical error of the sign is

$$\frac{\Delta \text{Sign}}{\langle \text{Sign} \rangle} = \frac{\sqrt{\langle \text{Sign}^2 \rangle - \langle \text{Sign} \rangle^2}}{\sqrt{N} \langle \text{Sign} \rangle} = \frac{\exp(\beta V \Delta f)}{\sqrt{N}}. \quad (3.3)$$

Here we have used $\text{Sign}^2 = 1$. To determine the average sign with sufficient accuracy one needs to generate on the order of $N = \exp(2\beta V \Delta f)$ configurations. For large volumes and small temperatures this is impossible in practice. It is possible to solve one half of the problem if one can match any contribution -1 with another contribution 1 to give 0 , such that only a few unmatched contributions 1 remain. Then effectively $\text{Sign} = 0, 1$ and hence $\text{Sign}^2 = \text{Sign}$. This reduces the relative error to

$$\frac{\Delta \text{Sign}}{\langle \text{Sign} \rangle} = \frac{\sqrt{\langle \text{Sign} \rangle - \langle \text{Sign} \rangle^2}}{\sqrt{N'} \langle \text{Sign} \rangle} = \frac{\exp(\beta V \Delta f / 2)}{\sqrt{N'}}. \quad (3.4)$$

One gains an exponential factor in statistics, but one still needs to generate $N' = \sqrt{N} = \exp(\beta V \Delta f)$ independent configurations in order to accurately determine the average sign.¹ This is because one generates exponentially many vanishing contributions before one encounters a contribution 1 . As explained below, in our cluster algorithm an explicit matching of contributions -1 and 1 is achieved using an improved estimator. This solves one half of the sign problem. In a second step involving a Metropolis decision, our algorithm ensures that contributions 0 and 1 occur with similar probabilities. This saves another exponential factor in statistics and solves the other half of the sign problem.

The meron-cluster fermion algorithm is based on a cluster algorithm for the corresponding bosonic model without the sign factor. Bosonic quantum spin systems

¹The fact that an improved estimator alone cannot solve the sign problem was pointed out to one of the authors by H. G. Evertz a long time ago.

can be simulated very efficiently with cluster algorithms [6, 7, 8]. The first cluster algorithm for lattice fermions was described in [9]. These algorithms can be implemented directly in the Euclidean time continuum [10], i.e. the Suzuki-Trotter discretization is not even necessary. The same is true for the meron-cluster algorithm. Here we discuss the algorithm for discrete time. The idea behind the algorithm is to decompose a configuration into clusters which can be flipped independently. Each lattice site belongs to exactly one cluster. When the cluster is flipped, the occupation number of all the sites on the cluster is changed from $n(x, t)$ to $1 - n(x, t)$, i.e. a cluster flip turns occupied into empty sites and vice versa. The decomposition of the lattice into clusters results from connecting neighboring sites on each individual space-time interaction plaquette following probabilistic cluster rules. A sequence of connected sites defines a cluster. In this case the clusters are sets of closed loops. The cluster rules are constructed to obey detailed balance. To show this we first write the plaquette Boltzmann factors as

$$\begin{aligned} \exp(-s[n(x, t), n(x + \hat{i}, t), n(x, t + 1), n(x + \hat{i}, t + 1)]) = \\ A\delta_{n(x, t), n(x, t+1)}\delta_{n(x+\hat{i}, t), n(x+\hat{i}, t+1)} + B\delta_{n(x, t), 1-n(x+\hat{i}, t)}\delta_{n(x, t+1), 1-n(x+\hat{i}, t+1)} + \\ C\delta_{n(x, t), n(x, t+1)}\delta_{n(x+\hat{i}, t), n(x+\hat{i}, t+1)}\delta_{n(x, t), 1-n(x+\hat{i}, t)} + D\delta_{n(x, t), n(x+\hat{i}, t+1)}\delta_{n(x+\hat{i}, t), n(x, t+1)} + \\ E\delta_{n(x, t), n(x, t+1)}\delta_{n(x+\hat{i}, t), n(x+\hat{i}, t+1)}\delta_{n(x, t), n(x+\hat{i}, t)}. \end{aligned} \quad (3.5)$$

The various δ -functions specify which sites are connected and thus belong to the same cluster. The quantities A, B, \dots, E determine the relative probabilities for different cluster break-ups of an interaction plaquette. We only allow break-ups which generate legal configurations under cluster flips. For example, A determines the probability with which sites are connected with their time-like neighbors, while B and D determine the probabilities for connections with space-like or diagonal neighbors, respectively. The quantities C and E determine the probabilities to put all four sites of a plaquette into the same cluster. This is possible for plaquette configurations $[0, 1, 0, 1]$ or $[1, 0, 1, 0]$ with a probability proportional to C and for configurations $[0, 0, 0, 0]$ or $[1, 1, 1, 1]$ with a probability proportional to E . The cluster rules are illustrated in table 1.

Inserting the expressions from eq.(2.12) one finds

$$\begin{aligned} \exp(-s[0, 0, 0, 0]) &= \exp(-s[1, 1, 1, 1]) = \exp(-\frac{\epsilon G}{2}) = A + D + E, \\ \exp(-s[0, 1, 0, 1]) &= \exp(-s[1, 0, 1, 0]) = \cosh \frac{\epsilon}{2} = A + B + C, \\ \exp(-s[0, 1, 1, 0]) &= \exp(-s[1, 0, 0, 1]) = \sinh \frac{\epsilon}{2} = B + D. \end{aligned} \quad (3.6)$$

For example, the probability to connect the sites with their time-like neighbors on a plaquette with configuration $[0, 0, 0, 0]$ or $[1, 1, 1, 1]$ is $A/(A + D + E)$, while the probability for a connection with their diagonal neighbor is $D/(A + D + E)$. All sites on such a plaquette are put into the same cluster with probability $E/(A + D + E)$. Similarly, the probability for connecting space-like neighbors on a plaquette with












weight	configuration	break-ups		
$\exp\left(-\frac{\epsilon G}{2}\right)$		 A	 D	 E
$\cosh\left(\frac{\epsilon}{2}\right)$		 A	 B	 C
$\sinh\left(\frac{\epsilon}{2}\right)$			 B	 D

Table 1: *Cluster break-ups of various plaquette configurations together with their relative probabilities A, B, \dots, E . The dots represent occupied sites and the fat lines are the cluster connections.*

configuration $[0, 1, 1, 0]$ or $[1, 0, 0, 1]$ is $B/(B + D)$ and the probability for diagonal connections is $D/(B + D)$.

Eq.(3.5) can be viewed as a representation of the original model as a random cluster model. The cluster algorithm operates in two steps. First, a cluster break-up is chosen for each space-time interaction plaquette according to the above probabilities. This effectively replaces the original Boltzmann weight of a plaquette configuration with a set of constraints represented by the δ -functions associated with the chosen break-up. The constraints imply that occupation numbers of connected sites can only be changed together. In the second step of the algorithm every cluster is flipped with probability $1/2$. When a cluster is flipped the occupation numbers of all sites that belong to the cluster are changed. Eq.(3.6) ensures that the cluster algorithm obeys detailed balance. To determine A, B, \dots, E we distinguish three cases. For $G \geq 1$ we solve eq.(3.6) by

$$A = \exp\left(-\frac{\epsilon G}{2}\right), \quad B = \sinh \frac{\epsilon}{2}, \quad C = \exp\left(-\frac{\epsilon}{2}\right) - \exp\left(-\frac{\epsilon G}{2}\right), \quad D = E = 0. \quad (3.7)$$

For $-1 \leq G \leq 1$ we use

$$\begin{aligned} A &= \frac{1}{2} \left[\exp\left(-\frac{\epsilon G}{2}\right) + \exp\left(-\frac{\epsilon}{2}\right) \right], \quad B = \frac{1}{2} \left[\exp\left(\frac{\epsilon}{2}\right) - \exp\left(-\frac{\epsilon G}{2}\right) \right], \quad C = 0, \\ D &= \frac{1}{2} \left[\exp\left(-\frac{\epsilon G}{2}\right) - \exp\left(-\frac{\epsilon}{2}\right) \right], \quad E = 0, \end{aligned} \quad (3.8)$$

and, finally, for $G \leq -1$

$$A = \cosh \frac{\epsilon}{2}, \quad B = C = 0, \quad D = \sinh \frac{\epsilon}{2}, \quad E = \exp(-\frac{\epsilon G}{2}) - \exp(\frac{\epsilon}{2}). \quad (3.9)$$

As an example, let us consider the antiferromagnetic quantum Heisenberg model, i.e. $G = 1$, and hence

$$A = \exp(-\frac{\epsilon}{2}), \quad B = \sinh \frac{\epsilon}{2}, \quad C = D = E = 0. \quad (3.10)$$

Consequently, on plaquette configurations $[0, 0, 0, 0]$ or $[1, 1, 1, 1]$ one always chooses time-like connections between sites, and for configurations $[0, 1, 1, 0]$ or $[1, 0, 0, 1]$ one always chooses space-like connections. For configurations $[0, 1, 0, 1]$ or $[1, 0, 1, 0]$ one chooses time-like connections with probability $p = A/(A + B) = 2/[1 + \exp(\epsilon/2)]$ and space-like connections with probability $1 - p = B/(A + B)$. Indeed, this is the algorithm that was used in [11]. It is extremely efficient, has almost no detectable autocorrelations, and its dynamical exponent for critical slowing down is compatible with zero.

Let us now consider the effect of a cluster flip on the fermion sign. It is obvious that the flip of a cluster either leads to a sign change or it leaves the sign unchanged. In general, the effect of the flip of a specific cluster on the fermion sign depends on the orientation of the other clusters. For example, a cluster whose flip does not change the sign now, may very well change the sign after other clusters have been flipped. In other words, the clusters affect each other in their effect on the fermion sign. This makes it very difficult to understand the effect of the various cluster flips on the topology of the fermion world-lines and thus on $\text{Sign}[n]$. As a consequence, for the most general model described above, we don't know how to solve the fermion sign problem. However, there are clusters whose effect on $\text{Sign}[n]$ is independent of the orientation of all the other clusters. Specifically, these are those clusters that do not contain any diagonal break-ups. To ensure that no clusters contain such break-ups we limit ourselves to models which have $D = 0$. According to eq.(3.7) this is the case for $G \geq 1$.

Once we forbid diagonal cluster break-ups, i.e. when $D = 0$, the clusters have a remarkable property with far reaching consequences: each cluster can then be characterized by its effect on the fermion sign independent of the orientation of all the other clusters. We refer to clusters whose flip changes $\text{Sign}[n]$ as merons, while clusters whose flip leaves $\text{Sign}[n]$ unchanged are called non-merons. The flip of a meron-cluster permutes the fermions and changes the topology of the fermion world-lines. The term meron has been used before to denote half-instantons. For example, the meron-clusters in the algorithm for the 2-d $O(3)$ model at non-zero vacuum angle θ are indeed half-instantons [12]. A configuration with an odd permutation of fermions has $\text{Sign}[n] = -1$ and can be viewed as an instanton, while a configuration with an even permutation of fermions is topologically trivial and has $\text{Sign}[n] = 1$. The flip of a meron-cluster changes an instanton into a topologically trivial

configuration and therefore is a half-instanton. In $(2 + 1)$ dimensions particles can have any statistics. The anyon statistics is characterized by a phase factor $\exp(i\theta H)$, where H is the integer-valued Hopf number. In that case, the flip of a meron-cluster changes the Hopf number by one, and the meron is indeed a half-Hopf-instanton. The number of merons in a configuration is always even. This follows when one considers flipping all clusters, and thus changing the occupation of all lattice sites, which leaves the fermion sign unchanged. If the number of merons would be odd, flipping all clusters would change the fermion sign, which implies that the number of merons must be even. An example of a meron-cluster is given in figure 2, which contains the same fermion configurations as figure 1. When the meron-cluster is flipped the first configuration with $\text{Sign}[n] = 1$ turns into the second configuration with $\text{Sign}[n] = -1$.

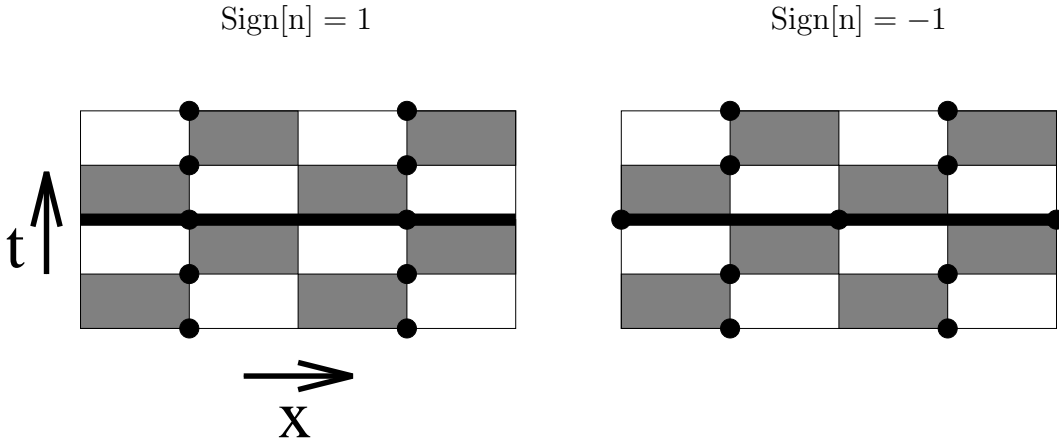


Figure 2: *The same fermion configurations as in figure 1 together with a meron-cluster represented by the fat line. The other clusters are not shown. Flipping the meron-cluster changes one configuration into the other and changes the fermion sign.*

The meron concept alone allows us to gain an exponential factor in statistics. Since all clusters can be flipped independently, one can construct an improved estimator for $\text{Sign}[n]$ by averaging analytically over the 2^{N_C} configurations obtained by flipping the N_C clusters in the configuration in all possible ways. For configurations that contain merons the average $\text{Sign}[n]$ is zero because flipping a single meron leads to a cancellation of contributions ± 1 . Hence, only the configurations without merons contribute to $\text{Sign}[n]$. The vast majority of configurations contains merons and now contributes an exact 0 to $\text{Sign}[n]$ instead of a statistical average of contributions ± 1 . In this way the improved estimator leads to an exponential gain in statistics.

Still, as it stands it is not guaranteed that the contributions from the zero-meron sector will always be positive. With no merons in the configuration it is clear that

the fermion sign remains unchanged under cluster flip, but one could still have $\text{Sign}[n] = -1$. Fortunately, there is a way to guarantee that $\text{Sign}[n] = 1$ in the zero-meron sector. In that case the contributions to $\text{Sign}[n]$ are 0 from configurations containing meron-clusters and 1 from configurations without merons. According to the previous discussion, this solves one half of the fermion sign problem. Let us describe how one can make sure that a configuration without merons always has $\text{Sign}[n] = 1$. This is possible when one does not allow the cluster break-ups characterized by the amplitudes D and E in eq.(3.5). This again limits us to models with $G \geq 1$, for which we have $D = E = 0$ according to eq.(3.7). The remaining cluster break-ups with amplitudes A, B, C have a very important property. They guarantee that sites inside a cluster obey a pattern of staggered occupation, i.e. either the even sites (with $x_1 + x_2 + x_3$ even) within the cluster are all occupied and the odd sites are all empty, or the even sites are all empty and the odd sites are all occupied. This guarantees that the clusters can be flipped such that one reaches the totally staggered reference configuration in which at all times all even sites are occupied and all odd sites are empty. In the corresponding antiferromagnet this configuration represents a completely ordered state with a staggered magnetization. In the half-occupied reference configuration (which is the first configuration in figure 1) all fermions are at rest, no fermions are permuted during the Euclidean time evolution, and thus $\text{Sign}[n] = 1$. Since any configuration can be turned into the reference configuration by appropriate cluster flips, this is particularly true for configurations without merons. Since the totally staggered configuration has $\text{Sign}[n] = 1$ and the fermion sign remains unchanged when a non-meron-cluster is flipped, all configurations without merons have $\text{Sign}[n] = 1$. Instead of a sequence of ± 1 for $\text{Sign}[n]$, we now have contributions 0 and 1. As discussed before, this only solves one half of the fermion sign problem. Before we can solve the other half of the problem we must discuss improved estimators for the physical observables.

Let us consider an improved estimator for $(\bar{\Psi}\Psi[n])^2 \text{Sign}[n]$ which is needed to determine the chiral susceptibility χ . The total chiral condensate, $\bar{\Psi}\Psi[n] = \sum_C \bar{\Psi}\Psi_C$, is a sum of cluster contributions

$$\bar{\Psi}\Psi_C = \frac{\epsilon}{6} \sum_{(x,t) \in C} (-1)^{x_1+x_2+x_3} (n(x,t) - \frac{1}{2}). \quad (3.11)$$

When a cluster is flipped, its condensate contribution changes sign. In a configuration without merons, where $\text{Sign}[n] = 1$ for all relative cluster flips, the average of $(\bar{\Psi}\Psi[n])^2 \text{Sign}[n]$ over all 2^{N_C} configurations is $\sum_C |\bar{\Psi}\Psi_C|^2$. For configurations with two merons the average is $2|\bar{\Psi}\Psi_{C_1}||\bar{\Psi}\Psi_{C_2}|$ where C_1 and C_2 are the two meron-clusters. Configurations with more than two merons do not contribute to $(\bar{\Psi}\Psi[n])^2 \text{Sign}[n]$. The improved estimator for the susceptibility is hence given by

$$\chi = \frac{\langle \sum_C |\bar{\Psi}\Psi_C|^2 \delta_{N,0} + 2|\bar{\Psi}\Psi_{C_1}||\bar{\Psi}\Psi_{C_2}| \delta_{N,2} \rangle}{V\beta \langle \delta_{N,0} \rangle}, \quad (3.12)$$

where N is the number of meron-clusters in a configuration. Thus, to determine χ one must only sample the zero- and two-meron sectors.

The probability to find a configuration without merons is exponentially small in the space-time volume since it is equal to $\langle \text{Sign} \rangle$. Thus, although we have increased the statistics tremendously with the improved estimators, without a second step one would still need an exponentially large statistics to accurately determine χ . Fortunately, the numerator in equation (3.12) receives contributions from the zero- and two-meron sectors only, while the denominator gets contributions only from the zero-meron sector. One can hence restrict oneself to the zero- and two-meron sectors and never generate configurations with more than two merons. This enhances both the numerator and the denominator by a factor that is exponentially large in the volume, but leaves the ratio of the two invariant. One purpose of the second step of the meron-cluster algorithm is to eliminate all configurations with more than two merons. To achieve this, we start with an initial configuration with zero or two merons. For example, a completely occupied configuration has no merons. We then visit all plaquette interactions one after the other and choose new pair connections between the four sites according to the above cluster rules. If the new connection increases the number of merons beyond two, it is not accepted and the old connection is kept for that plaquette. This procedure obeys detailed balance because configurations with more than two merons do not contribute to the observable we consider. This simple reject step eliminates almost all configurations with weight 0 and is the essential step to solve the other half of the fermion sign problem.

Assuming a dilute gas of meron and non-meron-clusters of typical space-time volume $|C|$ one finds a ratio $p(0)/p(2) \propto (|C|/V\beta)^2$ of the probabilities $p(0)$ and $p(2)$ to have zero or two merons. Hence, as long as the cluster size does not grow with the space-time volume, most configurations would have two merons and therefore would still have weight 0. Without further improvements, one would still need statistics quadratic (but no longer exponential) in the space-time volume to get an accurate average sign. The remaining problem can be solved with a reweighting technique similar to the one used in [12]. To enhance the zero-meron configurations in a controlled way, we introduce trial probabilities $p_t(0)$ and $p_t(2)$ which determine the relative weight of the zero- and two-meron sector. The trial distribution $p_t(N)$ for $N > 2$ is set to infinity. The distribution $p_t(N)$ is used in a Metropolis accept-reject step for the newly proposed pair connection on a specific plaquette interaction. A new pair connection that changes the meron number from N to N' is accepted with probability $p = \min[1, p_t(N)/p_t(N')]$. In particular, configurations with $N' > 2$ are never generated because then $p_t(N') = \infty$ and $p = 0$. After visiting all plaquette interactions, each cluster is flipped with probability 1/2 which completes one update sweep. After reweighting, the zero- and two-meron configurations appear with similar probabilities. This completes the second step in our solution of the fermion sign problem. The reweighting of the zero- and two-meron configurations is taken into account in the final expression for the chiral susceptibility as

$$\chi = \frac{\langle \sum_C |\bar{\Psi}\Psi_C|^2 \delta_{N,0} p_t(0) + 2 |\bar{\Psi}\Psi_{C_1}| |\bar{\Psi}\Psi_{C_2}| \delta_{N,2} p_t(2) \rangle}{V\beta \langle \delta_{N,0} p_t(0) \rangle}. \quad (3.13)$$

L	β	$\langle \text{Sign} \rangle$	$p_t(0)/p_t(2)$	$\langle \text{Sign} \rangle_r$	χ
4	0.6	0.838(1)	0.5/0.5	0.845(1)	0.554(1)
4	0.7	0.710(3)	0.5/0.5	0.726(2)	0.936(2)
4	0.8	0.534(4)	0.5/0.5	0.566(2)	1.678(5)
4	0.9	0.357(3)	0.5/0.5	0.405(2)	3.13(1)
4	0.948	0.282(2)	0.3/0.7	0.537(3)	4.22(2)
6	0.948	0.0556(7)	0.2/0.8	0.398(3)	9.83(8)
8	0.948	0.0020(4)	0.1/0.9	0.361(8)	16.6(5)
10	0.948	—	0.1/0.9	0.178(3)	26.5(8)
12	0.948	—	0.05/0.95	0.17(1)	37(1)
14	0.948	—	0.02/0.98	0.20(1)	51(1)
16	0.948	—	0.01/0.99	0.22(2)	65(2)

Table 2: Numerical results for the non-reweighted $\langle \text{Sign} \rangle$, the reweighted $\langle \text{Sign} \rangle_r$ and χ obtained with a reweighting factor $p_t(0)/p_t(2)$ on lattices of spatial size L at inverse temperature β . For the larger volumes the non-reweighted $\langle \text{Sign} \rangle$ is too small to be measured.

The optimal ratio $p_t(0)/p_t(2)$, which minimizes the statistical error of χ , can be estimated by gradually increasing the volume and the inverse temperature to their desired values.

4 Numerical Results

We have simulated the staggered fermion model with $G = 1$ on antiperiodic spatial volumes L^3 with $L = 4, 6, \dots, 16$ and at various inverse temperatures $\beta \in [0.5, 1.2]$ which includes the critical point. In the Euclidean time direction we have used $M = 4$, i.e. 24 time-slices. In all cases, we have performed at least 1000 thermalization sweeps followed by 10000 measurements. One sweep consists of a new choice of the cluster connections on each interaction plaquette and a flip of each cluster with probability $1/2$. To estimate an optimal ratio $p_t(0)/p_t(2)$ of the reweighting probabilities, we have first performed runs without reweighting. The observed relative probabilities of the zero- and two-meron sectors were used as an estimate for $p_t(0)/p_t(2)$ in production runs. Especially for the larger volumes, reweighting is necessary in order to obtain accurate results.

Some of our data for the chiral susceptibility χ are contained in table 2. The table also includes the non-reweighted $\langle \text{Sign} \rangle$, the value of the used reweighting factor $p_t(0)/p_t(2)$ as well as the reweighted $\langle \text{Sign} \rangle_r$. Note that $\langle \text{Sign} \rangle_r$ is the fraction of zero-meron configurations that the algorithm generates by sampling the zero-

and two-meron sectors only. This quantity is typically a lot bigger than the original non-reweighted $\langle \text{Sign} \rangle$, which is the fraction of zero-meron configurations in the space of all configurations including those with many merons. In particular, in large space-time volumes the staggered fermion model suffers from a very severe sign problem. Figure 3 shows the probability to have a certain number of merons

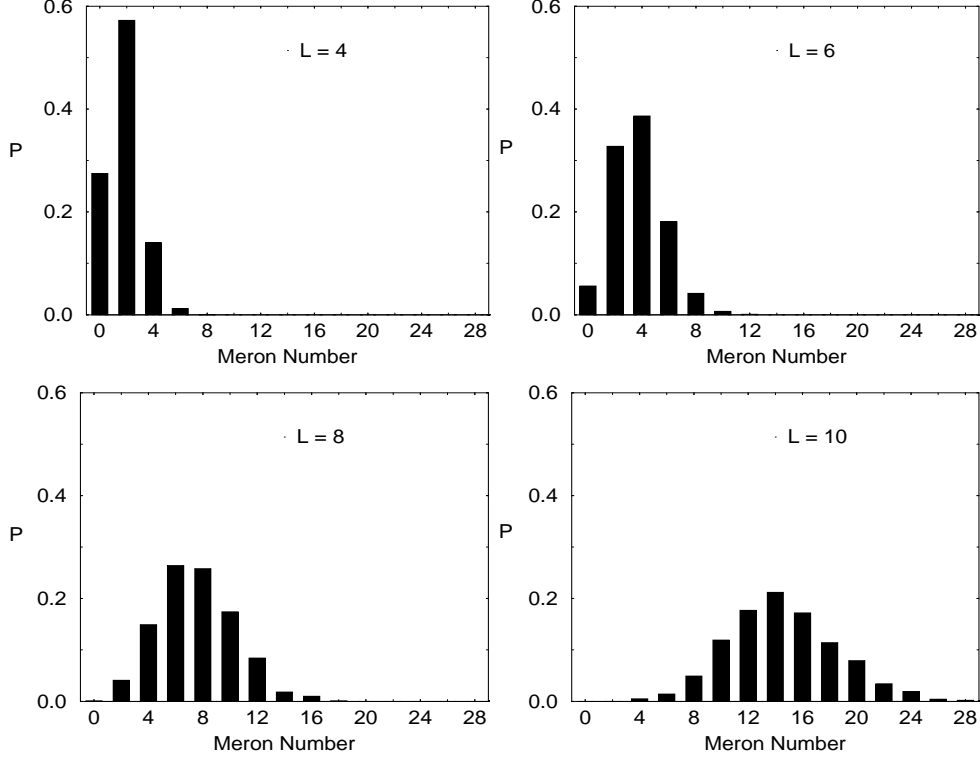


Figure 3: *The probability of having a certain number of merons for various spatial sizes $L = 4, 6, 8$ and 10 at $\beta = 0.948$.*

in an algorithm that samples all meron-sectors without reweighting. For small volumes the zero-meron sector and hence $\langle \text{Sign} \rangle$ are relatively large, while multi-meron configurations are rare. On the other hand, in larger volumes the vast majority of configurations has a large number of merons and hence $\langle \text{Sign} \rangle$ is exponentially small. For example, an extrapolation from smaller volumes gives a rough estimate for the non-reweighted $\langle \text{Sign} \rangle \approx 10^{-20}$ on the 16^3 lattice at $\beta = 0.948$, while the reweighted $\langle \text{Sign} \rangle_r = 0.22(2)$. Hence, to achieve a similar accuracy without the meron-cluster algorithm one would have to increase the statistics by a factor 10^{40} , which is obviously impossible in practice. In fact, at present there is no other method that can be used to simulate this model.

Figure 4 shows the chiral susceptibility χ as a function of β for various spatial sizes L . At high temperatures (small β) χ is almost independent of the volume, in-

dicating that chiral symmetry is unbroken. On the other hand, at low temperatures χ increases with the volume, which implies that chiral symmetry is spontaneously broken. To study the critical behavior in detail, we have performed a finite-size

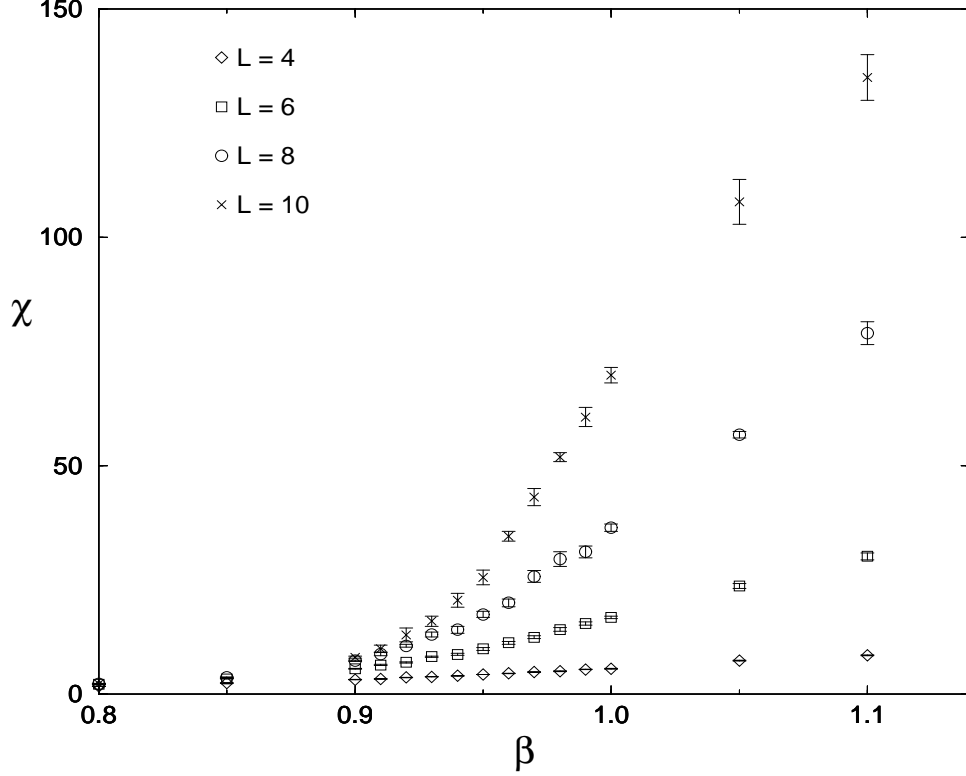


Figure 4: *The chiral susceptibility χ as a function of the inverse temperature β for various spatial sizes $L = 4, 6, 8$ and 10 .*

scaling analysis for χ focusing on a narrow range $\beta \in [0.9, 0.98]$ around the critical point. Since a $\mathbf{Z}(2)$ chiral symmetry gets spontaneously broken at finite temperature in this $(3+1)$ -d model, one expects to find the critical behavior of the 3-d Ising model. The corresponding finite-size scaling formula valid close to β_c is [13]

$$\begin{aligned}\chi(L, \beta) &= a(x) + b(y)L^{\gamma/\nu}, \\ a(x) &= a_0 + a_1x + a_2x^2 + \dots, \quad x = \beta - \beta_c, \\ b(y) &= b_0 + b_1y + b_2y^2 + \dots, \quad y = (\beta - \beta_c)L^{1/\nu}.\end{aligned}\tag{4.1}$$

For the 3-d Ising model the critical exponents are given by $\nu = 0.630(1)$ and $\gamma/\nu = 1.963(3)$ [13]. Fitting our data, we find $\nu = 0.63(4)$ and $\gamma/\nu = 1.98(2)$, which indicates that the chiral transition of the staggered fermion model is indeed in the 3-d Ising universality class. The fit gives $\beta_c = 0.948(3)$. In figure 5 we have taken the values of the critical exponents from the 3-d Ising model, and we have plotted $\chi/L^{\gamma/\nu}$ as a function of $y = (\beta - \beta_c)L^{1/\nu}$. For large enough L one can neglect the

term $a(x)$ in eq.(4.1) and one obtains $\chi/L^{\gamma/\nu} = b(y)$. We have varied the value of β_c and found that indeed all data can be collapsed on one universal curve. The resulting critical inverse temperature is $\beta_c = 0.948(3)$ in agreement with the previous fit. At the estimated value of β_c , we have performed simulations on larger spatial

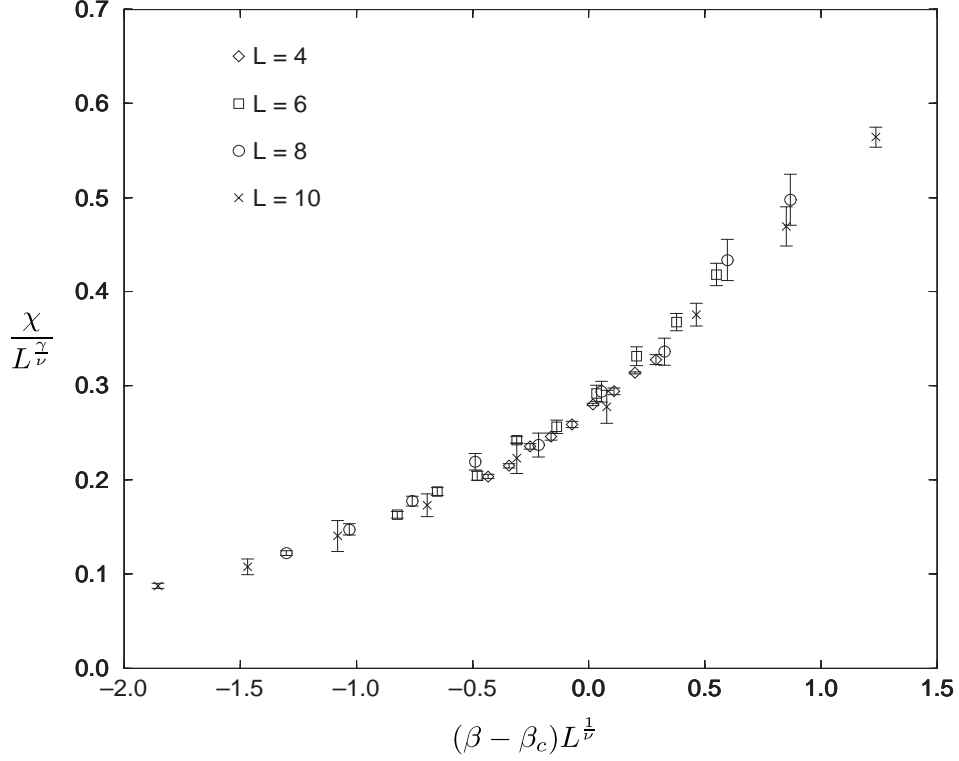


Figure 5: *Finite-size scaling behavior of the chiral susceptibility χ . The data for various spatial sizes $L = 4, 6, 8$ and 10 fall on one universal curve.*

volumes up to 16^3 . The results for χ are shown in figure 6 together with a fit that gives an independent estimate of $\gamma/\nu = 1.98(2)$. All of this supports the claim that the chiral transition in our model is Ising-like.

5 Conclusions

We have applied a new fermion simulation technique — the meron-cluster algorithm — to a model of staggered fermions. In contrast to standard methods which integrate out the fermions and are left with a non-local bosonic action, we describe the fermions in a Fock state occupation number basis and thus keep a local bosonic action. The fermion permutation sign arises due to the Pauli exclusion principle as a non-local factor associated with non-trivial topology of the fermion world-lines.

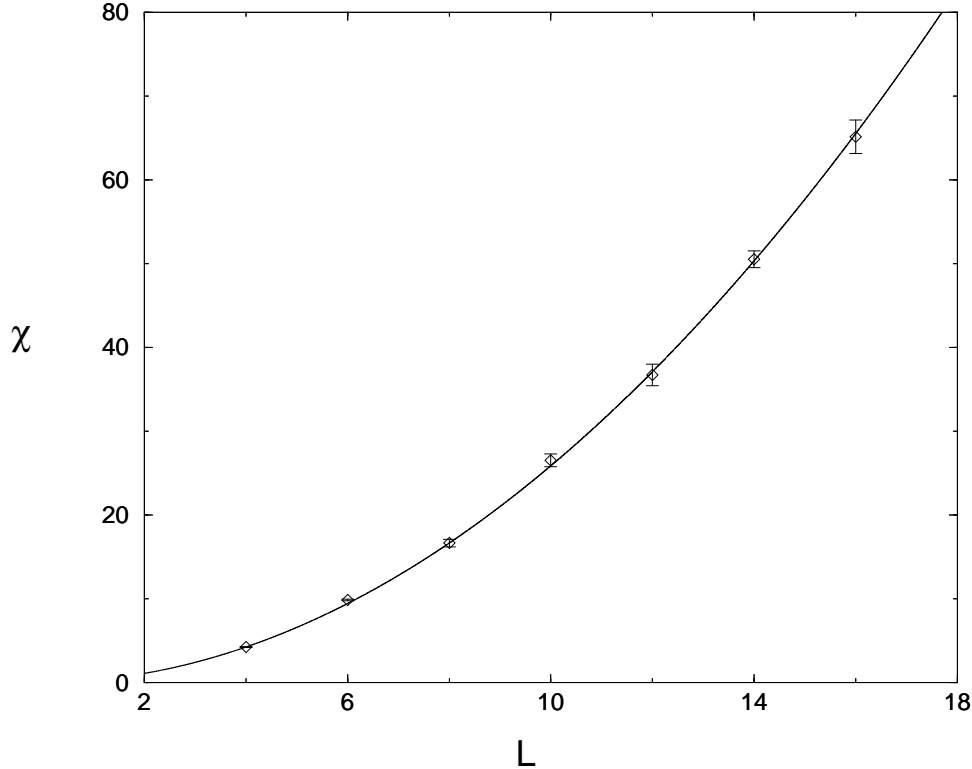


Figure 6: *Finite-size scaling behavior of the chiral susceptibility χ as a function of the spatial size L at the estimated critical inverse temperature $\beta_c = 0.948$. A fit of the volume-dependence (solid line) gives the critical exponent $\gamma/\nu = 1.98(2)$ of the 3-d Ising model.*

The sign leads to severe cancellations which makes standard simulation techniques impossible to use. The decomposition of a configuration into clusters allows us to disentangle the complicated topology of the fermion world-lines. In particular, a meron-cluster identifies a pair of configurations with equal weight and opposite sign. This results in an explicit cancellation of two contributions ± 1 to the path integral, such that only the zero-meron sector contributes to the partition function. Observables like the chiral susceptibility χ receive contributions only from the zero- and two-meron sectors. To measure χ one can hence eliminate all sectors with more than two merons, which leads to an exponential gain in statistics and to a complete solution of the fermion sign problem.

The meron-cluster algorithm allowed us to simulate a staggered fermion model for which standard fermion methods suffer from a severe sign problem. The model has two flavors and a $\mathbf{Z}(2)$ chiral symmetry which is spontaneously broken at low temperatures. Applying finite-size scaling methods to the high-precision numerical data for the chiral susceptibility, we extracted critical exponents compatible with those of the 3-d Ising model. This is the expected behavior based on universality

arguments and dimensional reduction. It would be interesting to apply our method to (2+1) dimensions. The $N = 4$ flavor case was studied in [2] and it was verified that the model is in the 2-d Ising universality class. The standard fermion algorithm that was used in that study does not work for $N < 4$ due to the fermion sign problem. The meron-cluster algorithm solves the sign problem and can be used to explore those models.

Even in cases without a sign problem, the meron-cluster algorithm is more efficient than standard fermion simulation methods. However, one should keep in mind that the meron-cluster algorithm is not always applicable. For example, the meron concept applies only when the clusters are independent in their effect on the fermion sign. In addition, it must always be possible to flip the clusters such that one reaches a reference configuration with a positive sign. Otherwise, some contributions from the zero-meron sector could be negative. For example, in our model these restrictions led to $G \geq 1$, i.e. to a sufficiently strong four-fermion coupling. In this paper, we have not attempted to take the continuum limit of the lattice theory. Instead, we have studied the chiral phase transition at a finite lattice spacing corresponding to $G = 1$. The restriction $G \geq 1$ would prevent us from approaching the continuum limit if it corresponds to $G_c < 1$. It should be pointed out that we can study the universal behavior of the chiral transition without taking the continuum limit. Of course, it is not excluded that appropriate modifications of the algorithm might allow us to work at $G < 1$.

A natural arena for applications of the meron-cluster algorithm are quantum link models [14] which are used in the D-theory formulation of QCD [15, 16, 17]. In D-theory continuous classical fields arise from the dimensional reduction of discrete quantum variables. In these models the continuum limit is approached by varying the extent of an extra dimension, not by varying the value of a bare coupling constant. Hence, restrictions such as $G \geq 1$ would not prevent us from taking the continuum limit. In quantum link QCD the quarks arise as domain wall fermions. The application of meron-cluster algorithms to domain wall fermions is in progress. Also there are many applications to sign problems in condensed matter physics. Investigations of antiferromagnets in a magnetic field and of systems in the Hubbard model family will be reported elsewhere.

At present, the meron-cluster algorithm is the only method that allows us to solve the fermion sign problem. A severe sign problem arises in lattice QCD calculations at non-zero baryon number due to a complex action. It is therefore natural to ask if our algorithm can be applied to this case. At non-zero chemical potential the 2-d $O(3)$ model, which is a toy model for QCD, also suffers from a sign problem due to a complex action. When applied to the D-theory formulation of this model, the meron-cluster algorithm solves the sign problem completely. It remains to be seen if a similar result can be achieved for QCD.

Acknowledgements

S. C. likes to thank M.I.T. and U.-J. W. likes to thank Duke University for hospitality. We have benefitted from discussions about cluster algorithms with R. C. Brower, H. G. Everts and M. Troyer. U.-J. W. also likes to thank the A. P. Sloan foundation for its support.

References

- [1] J. B. Kogut, M. A. Stephanov and C. G. Strouthos, Phys. Rev. D58 (1998) 096001.
- [2] J. B. Kogut and C. G. Strouthos, hep-lat/9904008.
- [3] S. Chandrasekharan and U.-J. Wiese, cond-mat/9902128.
- [4] L. Susskind, Phys. Rev. D16 (1977) 3031.
- [5] P. Jordan and E. Wigner, Z. Phys. 47 (1928) 631.
- [6] U.-J. Wiese and H.-P. Ying, Phys. Lett. A168 (1992) 143.
- [7] H. G. Evertz, G. Lana and M. Marcu, Phys. Rev. Lett. 70 (1993) 875.
- [8] H. G. Evertz, The loop algorithm, in Numerical Methods for Lattice Quantum Many-Body Problems, ed. D. J. Scalapino, Addison-Wesley Longman, Frontiers in Physics
- [9] U.-J. Wiese, Phys. Lett. B311 (1993) 235.
- [10] B. B. Beard and U.-J. Wiese, Phys. Rev. Lett. 77 (1996) 5130.
- [11] U.-J. Wiese and H.-P. Ying, Z. Phys. B93 (1994) 147.
- [12] W. Bietenholz, A. Pochinsky and U.-J. Wiese, Phys. Rev. Lett. 75 (1995) 4524.
- [13] H. W. J. Blöte, E. Luitjen and J. R. Heringa, J. Phys. A28 (1995) 6289.
- [14] S. Chandrasekharan and U.-J. Wiese, Nucl. Phys. B492 (1997) 455.
- [15] R. C. Brower, S. Chandrasekharan and U.-J. Wiese, hep-th/9704106, to appear in Phys. Rev. D.
- [16] B. B. Beard, R. C. Brower, S. Chandrasekharan, D. Chen, A. Tsapalis and U.-J. Wiese, Nucl. Phys. B (Proc. Suppl.) 63 (1998) 775.
- [17] U.-J. Wiese, Nucl. Phys. B (Proc. Suppl.) 73 (1999) 146.